Compact Assumption Applied to the Monopole Term of Farassat's Formulations

Leonard V. Lopes*

Abstract

Farassat's formulations provide an acoustic prediction at an observer location provided a source surface, including motion and flow conditions. This paper presents compact forms for the monopole term of several of Farassat's formulations. When the physical surface is elongated, such as the case of a high aspect ratio rotorcraft blade, compact forms can be derived which are shown to be a function of the blade cross sectional area by reducing the computation from a surface integral to a line integral. The compact forms of all formulations are applied to two example cases: a short span wing with constant airfoil cross section moving at three forward flight Mach numbers and a rotor at two advance ratios. Acoustic pressure time histories and power spectral densities of monopole noise predicted from the compact forms of all the formulations at several observer positions are shown to compare very closely to the predictions from their non-compact counterparts. A study on the influence of rotorcraft blade shape on the high frequency portion of the power spectral density shows that there is a direct correlation between the aspect ratio of the airfoil and the error incurred by using the compact form. Finally, a prediction of pressure gradient from the non-compact and compact forms of the thickness term of Formulation G1A shows that using the compact forms results in a 99.6% improvement in computation time, which will be critical when noise is incorporated into a design environment.

Nomenclature

English:

c	speed of sound
f	integration surface defined by $f = 0$
f	integration line (quarter chord)
F_i	compact line dipole source term
J	Jacobian transformation of surface
$H(x)$	Heaviside function
K	Jacobian transformation of line
L_i	surface dipole source term
M	Mach number
n_i	outward directed unit normal vector
p'	acoustic pressure
p_{ij}	compressive stress tensor
Q	monopole source term
r	radiation vector
t	observer time
T_{ij}	quadrupole source term
u	time-independent coordinate of line
u_1, u_2	time-independent coordinate of surface
u_i, v_i	flow and surface velocity

Greek:

$\delta(x)$	Dirac delta function
δ_{ij}	Kronecker delta
Λ	airfoil cross section
Φ	acoustic velocity potential
Ψ	volume enclosed by $f = 0$, $\Psi = \Lambda * K$
ρ	fluid density
τ	retarded time

Subscript:

m	monopole term
M	Mach direction
n	unit normal direction
r	radiation direction
∞	freestream quantity

Superscript:

$\dot{}$	source time derivative
$'$	perturbation quantity
$\bar{}$	generalized derivative

Symbol:

$\Box^2$	wave operator, $1/c_\infty^2 \, \partial^2/\partial t^2 - \partial^2/\partial x_i \partial x_j$

*Research Aerospace Engineer; NASA Langley Aeroacoustics Branch, Member AIAA; leonard.v.lopes@nasa.gov

I. Introduction

Community noise has been an ongoing problem for aircraft and is projected to be a major concern in the future due to increased air traffic.[1] Both conventional and unconventional aircraft designs continue to be evaluated,[2,3] in which assessments are performed using aircraft noise prediction and measured data if available. Aircraft designs increasingly include acoustics in the design process, and therefore require many estimations of the noise without the fine detail that is required to do an in-depth acoustic assessment. This leads to the requirement of lower-order noise predictions based on assumptions that provide not only an estimation of the noise, but can include trends and error estimation as well, all with a quick turnaround time.

NASA initiated the development of the Aircraft NOise Prediction Program (ANOPP)[4,5] approximately 40 years ago to provide the U.S. Government with the ability to assess aircraft noise. The prediction methodologies that have been implemented within ANOPP were developed as empirical or semi-empirical models, using the best available experimental data sets and acoustic prediction methods. Recently, NASA developed the second generation Aircraft NOise Prediction Program (ANOPP2).[6] ANOPP2, while including ANOPP's capability and history, pushes the bounds of noise prediction by allowing for a mixed-fidelity noise computation, one that allows for higher-order methods to be combined with lower-order methods in a unified system, specifically for design. This mixed-fidelity design is beneficial when integrating acoustics into a multi-disciplinary environment such as Phoenix Integration's ModelCenter® or NASA's OpenMDAO,[7] and effort has begun on that front. Meanwhile, methods can be implemented into ANOPP2 that can predict the noise based on lower-order algorithms for certain types of applications. One such application is rotorcraft noise.

Rotorcraft noise can be estimated by several techniques, including those based on field measurements and computations, and can be separated into two terms: the monopole (or thickness) term and the dipole (or loading) term (the quadrupole term is not considered here). The monopole term is caused by the displacement of the medium as the blade moves through the atmosphere, and the dipole term is caused by the force that is exerted by the blade. The information required to predict the monopole term includes the blade geometrical properties and its motion, while the information required to predict the dipole term also includes the surface pressures on the blade. The blade surface pressures for rotorcraft are challenging to predict due to the complex blade motions (including blade deformation), blade-wake interactions, high tip speeds, and complicated near-field flow features due to the proximity of the rotorcraft body. Once the pressure on the blades is determined, the noise can be predicted using Farassat's Formulation 1A[8] which assumes a uniform stationary medium and applies a free-space Green's function to propagate the noise from the source to the observer. When using comprehensive codes, such as CAMRAD II,[9] that provide a lifting line coinciding with the rotor blade, a compact form of the dipole term can be used to predict the dipole component of the noise. However, the same compact assumption technique cannot be directly applied to the monopole term, and previous analyses include a non-compact monopole term combined with a compact dipole term.[10]

Recently, there has been an effort to apply the compact assumption to the monopole term.[11] This compact assumption of the monopole term, called the dual-compact loading approach, relies on a formulation by Isom[12] and has been shown to be effective in understanding in-plane rotor noise and reducing computation time compared to non-compact forms. However, the compact assumption presented in Ref. 11 is only applied to Formulation 1A and is dependent on the placement of the dual compact lines, both of which require computations, effectively doubling a single line computation such as in the compact dipole noise term.

This paper introduces compact forms of the monopole term of several of Farassat's formulations based on an identity introduced by Succi.[13] Section II will show the derivation of the compact assumption when applied to the monopole term of three types of formulations: acoustic pressure, pressure gradient, and acoustic velocity. Section III will demonstrate the compact forms of the formulations by applying them to two example cases: a short span wing segment undergoing constant forward flight and a rotorcraft at two advance ratios. Section IV will explore the effect of blade shape on high frequency fall off rate and estimate error incurred when utilizing the compact assumption. Finally, Section V demonstrates the computational efficiency by applying the compact assumption to a rotor near a body.

II. Compact Monopole Formulations

The derivation of the Ffowcs Williams and Hawkings (FW-H) equation[14] uses generalized function theory[15] and Lighthill's stress tensor[16,17] to define the acoustic pressure caused by a noise-generating mechanism. The FW-H equation, Eq. 1, includes two surface source terms and one volume source term. The surface source terms are identified by the delta function, $\delta(x)$, and the volume source term is identified by the Heaviside function, $H(x)$. The source terms on the right hand side of the FW-H equation often are called the monopole, dipole, and quadrupole terms respectively. The surface f, shown in Fig. 1, can be impermeable, such as a rotor blade surface, or permeable, such as a computational surface surrounding the entire rotor. The general source terms are shown in Eq. 2, and the simplified source terms valid for impermeable surfaces are shown in Eq 3. Both forms of the FW-H equation are used frequently with a Computational Fluid Dynamics (CFD) solution which provides the flow properties. The CFD solution calculates the near-field hydrodynamics, acoustic generation, and acoustic propagation inside the surface, and the FW-H equation uses the information on the surface to propagate the noise to the observer. Integral solutions of the FW-H equation, often assuming a free space Green's function, represent the noise propagation from the surface to an observer location in the near- or far-field. The CFD/FW-H approach has been applied to many different types of geometries such as helicopter rotors, open rotors, landing gear, slats, flaps, trailing edges, jets, and wind turbines.[18–24]

$$\bar{\Box}^2 p' = \frac{\partial}{\partial t}\{Q\delta(f)\} - \frac{\partial}{\partial x_i}\{L_i\delta(f)\} + \frac{\bar{\partial}^2}{\partial x_i \partial x_j}\{T_{ij}H(f)\} \tag{1}$$

$$Q = \rho_\infty v_n + \rho(u_n - v_n), \qquad L_i = p_{ij}n_j + \rho u_i(u_n - v_n), \qquad T_{ij} = \rho u_i u_j + p_{ij} - c_\infty^2 \rho' \delta_{ij} \tag{2}$$

$$Q = \rho_\infty v_n, \qquad L_i = p_{ij}n_j, \qquad T_{ij} = \rho u_i u_j + p_{ij} - c_\infty^2 \rho' \delta_{ij} \tag{3}$$

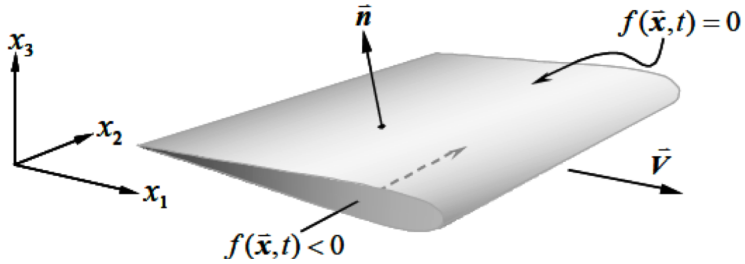

Figure 1. Description of a surface in motion by $f(\mathbf{x},t)=0$, $\bar{n}=\frac{\partial f}{\partial \mathbf{x}}$, $f(\mathbf{x},t)<0$ inside the surface, and $f(\mathbf{x},t)>0$ outside the surface.

There are several solutions to the FW-H equation proposed by Farassat, including the most frequently used Formulation 1A.[8] During his time in the Aeroacoustics Branch at the NASA Langley Research Center, Farassat[25] proposed that any general solution to the FW-H equation satisfy the following requirements which are taken verbatim from Ref. 25:

1. There must be no restrictions on the geometry of the noise generator (blades, airframe, etc.). This means that results for a flat (infinitely thin) plate are not acceptable.

2. There must be no restrictions on the kinematics of the noise generator. This means that the motion of the source cannot be restricted to lie on a straight line or a helicoidal surface.

3. The result must be valid in the near and far fields.

4. One should be able to calculate the noise for an observer that is stationary in the medium, or in motion with the aircraft.

Once a derivation has been developed using the above assumptions, any deviation that violates one of the assumptions is a subset of the more general solution. In the current analysis, the compact assumption is applied to the monopole term of several formulations. The dipole is not addressed here, and the quadrupole term is excluded from all of Farassat's Formulations by definition. The compact assumption breaks the first

and third constraint, and therefore, any solution presented here is a compact form of an existing formulation, not a new formulation. Even though the compact form of the dipole term of Formulation 1A has been utilized extensively, to the authors knowledge, the compact forms of the other Formulations have not been published. For completeness, the dipole term of the compact form of each of the formulations included here is listed in the Appendix. It is worth noting that the compact forms of the dipole term do not follow the same derivation presented here, but only utilizes the compact assumption as it applies to the frequency of the pressure fluctuations on the surface and the ratio of chord length to radiation distance.

Derivation

Following a derivation from Farassat,[8] the noise from the monopole term is the solution of the following:

$$\bar{\Box}^2 p'_m(x_i,t) = \frac{\partial}{\partial t}\Big[\rho_\infty v_n |\nabla f| \delta(f)\Big] \tag{4}$$

where $f = 0$ is the surface. The surface can be written as a volume of sources by recognizing that the rate of change of the volume enclosed by the surface is relatable to the velocity of the surface, shown by Eq. 5.[13]

$$\frac{\partial}{\partial t}\Big[1 - H(f)\Big] = v_n |\nabla f| \delta(f) \tag{5}$$

Therefore, the monopole term is proportional to the second derivative with respect to time of the volume encapsulated by the surface.

$$\bar{\Box}^2 p'_m(x_i,t) = \rho_\infty \frac{\partial^2}{\partial t^2}\Big[1 - H(f)\Big] \tag{6}$$

Using a free space Green's function, the acoustic pressure at the observer location is a function of the volume encapsulated by the retarded surface (Σ-surface) and the distance from the volume to the observer location ($r(x_i,t;y_i,\tau) = |x_i(t) - y_i(\tau)|$). Assuming an elongated body, such as a rotor blade, and applying a geometrically compact assumption ($r_{min} \gg$ blade chord), the monopole term can be reduced to an integration along a line of the cross sectional area (Λ), where $d\mathbf{L}$ is the differential length of the compact line placed at the quarter chord defined by f = 0.

$$4\pi p'_m(x_i,t) = \rho_\infty \frac{\partial^2}{\partial t^2}\int_{f<0}\left[\frac{1}{r|1-M_r|}dy\right]_{ret} \approx \rho_\infty \frac{\partial^2}{\partial t^2}\int_{\mathrm{f}=0}\left[\frac{\Lambda}{r|1-M_r|}\right]_{ret} d\mathbf{L} \tag{7}$$

Equation 7 is the starting point for the compact forms of Farassat's formulations derived in this paper. The derivations are simplified by using a shorthand notation introduced by Lee[26] and include deformation of the source surface and compact line,[27] outlined in Eq. 8.

$$R(n,m) = r^{-n}(1-M_r)^{-m} \qquad d\mathbf{S} = J du_1 du_2 \qquad d\mathbf{L} = K du \tag{8}$$

Using the above shorthand notation, Eq. 7 is reformulated as

$$\frac{4\pi}{\rho_\infty} p'_m(x_i,t) = \frac{\partial^2}{\partial t^2}\int_{\mathrm{f}=0}\Big[\Lambda K R(1,1)\Big]_{ret} du \tag{9}$$

In the following sections, the compact and non-compact forms of the formulations implemented in ANOPP2[6] are shown. These are broken down into three groups: pressure formulations, pressure gradient formulations, and velocity formulations. The pressure formulations include Formulation 1, 1A, and 2B. The pressure gradient formulations include Formulation G0, G1, and G1A. And finally, the velocity formulation is Formulation V1A. Each formulation is accompanied by a set of coefficients that simplify the equation. These are denoted by subscript, for example A_{1A} is the first coefficient of Formulation 1A. The coefficients that accompany the non-compact forms are in equation type face (A_{1A}) and the compact counterpart is in text type face (A_{1A}).

A. Pressure Formulations

Equation 10 is the non-compact form of Formulation 1 taken directly from Farassat.[8] Using the derivation outlined in the previous section, the compact form of the monopole term of Formulation 1 is Eq. 11

$$4\pi p_m(x_i,t) = \frac{\partial}{\partial t}\int_{f=0}\left[(QJ)A_1\right]_{ret} du_1 du_2 \tag{10}$$

$$A_1 = R(1,1)$$

$$\frac{4\pi}{\rho_\infty} p_m(x_i,t) = \frac{\partial^2}{\partial t^2}\int_{\mathrm{f}=0}\left[(\Lambda K)\mathrm{A}_1\right]_{ret} du \tag{11}$$

$$\mathrm{A}_1 = R(1,1)$$

Applying the identity $\partial/\partial t = R(0,1)\partial/\partial\tau$, the non-compact form of Formulation 1A is shown in Eq. 12 and the compact form is Eq. 13.

$$4\pi p_m(x_i,t) = \int_{f=0}\left[(\dot{Q}J + Q\dot{J})A_{1A} + (QJ)B_{1A}\right]_{ret} du_1 du_2 \tag{12}$$

$$A_{1A} = R(0,1)A_1 \qquad B_{1A} = R(0,1)\dot{A}_1$$

$$\frac{4\pi}{\rho_\infty} p_m(x_i,t) = \int_{\mathrm{f}=0}\left[(\ddot{\Lambda}K + 2\dot{\Lambda}\dot{K} + \Lambda\ddot{K})\mathrm{A}_{1A} + (\dot{\Lambda}K + \Lambda\dot{K})\mathrm{B}_{1A} + (\Lambda K)\mathrm{C}_{1A}\right]_{ret} du \tag{13}$$

$$\mathrm{A}_{1A} = R(0,2)\mathrm{A}_1 \qquad \mathrm{B}_{1A} = R(0,2)\dot{\mathrm{A}}_1 + R(0,1)\dot{R}(0,1)\mathrm{A}_1$$

$$\mathrm{C}_{1A} = R(0,2)\ddot{\mathrm{A}}_1 + R(0,1)\dot{R}(0,1)\dot{\mathrm{A}}_1$$

Formulation 2B is a broadband formulation proposed by Farassat and Casper[25] that computes the acoustic pressure spectrum via the velocity potential Φ. The non-compact and compact forms of monopole component of Formulation 2B are shown in Eq. 14 and 16, respectively.

$$\hat{p}'(x_i,f) = -2\pi i f \rho_\infty \hat{\Phi}(x_i,f) \tag{14}$$

$$4\pi\rho_\infty \Phi_m = -\int_{f=0}\left[(QJ)A_{2B}\right]_{ret} du_1 du_2 \tag{15}$$

$$A_{2B} = R(1,1)$$

$$4\pi\Phi_m(x_i,t) = -\frac{\partial}{\partial t}\int_{\mathrm{f}=0}\left[(\Lambda K)\mathrm{A}_{2B}\right]_{ret} du \tag{16}$$

$$\mathrm{A}_{2B} = R(1,1)$$

B. Pressure Gradient Formulations

Pressure gradient formulations are used in conjunction with scattering algorithms, such as the FAST scattering code,[28] to account for scattering and shielding of noise caused by an object, such as an aircraft, in proximity to the sound source. Pressure gradient formulations provide the incident field on the scattering body and at the observer while the scattering codes provide the scattered field.[26] The sum of the incident and scattered fields is then the total noise at the observer. There are currently three pressure gradient formulations implemented in ANOPP2: Formulation G0, G1, and G1A. The non-compact and compact forms of Formulation G0 are shown in Eq. 17 and 18, respectively.

$$4\pi c_\infty \frac{\partial p'_m}{\partial x_i}(x_i,t) = -\frac{\partial^2}{\partial t^2}\int_{f=0}\left[(QJ)A_{G0,i}\right]_{ret} du_1 du_2 - \frac{\partial}{\partial t}\int_{f=0}\left[(QJ)B_{G0,i}\right]_{ret} du_1 du_2 \tag{17}$$

$$A_{G0,i} = R(1,1)\hat{r}_i \qquad B_{G0,i} = c_\infty R(2,1)\hat{r}_i$$

$$4\pi\frac{c_\infty}{\rho_\infty}\frac{\partial p'_m}{\partial x_i}(x_i,t) = -\frac{\partial^3}{\partial t^3}\int_{\mathrm{f}=0}\left[(\Lambda K)\mathrm{A}_{G0,i}\right]_{ret} du - \frac{\partial^2}{\partial t^2}\int_{\mathrm{f}=0}\left[(\Lambda K)\mathrm{B}_{G0,i}\right]_{ret} du \tag{18}$$

$$\mathrm{A}_{G0,i} = R(1,1)\hat{r}_i \qquad \mathrm{B}_{G0,i} = c_\infty R(2,1)\hat{r}_i$$

The non-compact and compact forms of the monopole component of Formulation G1 are shown in Eq. 19 and 20, respectively.

$$4\pi c_\infty \frac{\partial p'_m}{\partial x_i}(x_i,t) = -\frac{\partial}{\partial t}\int_{f=0}\left[(\dot{Q}J + Q\dot{J})A_{G1,i} + (QJ)B_{G1,i}\right]_{ret} du_1 du_2 \tag{19}$$

$$A_{G1,i} = R(0,1)A_{G0,i} \qquad B_{G1,i} = R(0,1)\dot{A}_{G0,i} + B_{G0,i}$$

$$4\pi \frac{c_\infty}{\rho_\infty}\frac{\partial p'_m}{\partial x_i}(x_i,t) = -\frac{\partial}{\partial t}\int_{\mathrm{f}=0}\left[(\ddot{\Lambda}K + 2\dot{\Lambda}\dot{K} + \Lambda\ddot{K})\mathrm{A}_{G1,i} + (\dot{\Lambda}K + \Lambda\dot{K})\mathrm{B}_{G1,i} + (\Lambda K)\mathrm{C}_{G1,i}\right]_{ret} du \tag{20}$$

$$\mathrm{A}_{G1,i} = R(0,2)\mathrm{A}_{G0,i} \qquad \mathrm{B}_{G1,i} = R(0,1)(\dot{R}(0,1)\mathrm{A}_{G0,i} + \mathrm{B}_{G0,i})$$

$$\mathrm{C}_{G1,i} = R(0,2)\ddot{\mathrm{A}}_{G0,i} + R(0,1)\dot{R}(0,1)\dot{\mathrm{A}}_{G0,i} + R(0,1)\dot{\mathrm{B}}_{G0,i}$$

And finally, the non-compact and compact forms of monopole component of Formulation G1A are shown in Eq. 21 and 22, respectively.

$$4\pi c_\infty \frac{\partial p'_m}{\partial x_i}(x_i,t) = -\int_{f=0}\left[(\ddot{Q}J + 2\dot{Q}\dot{J} + Q\ddot{J})A_{G1A,i} + (\dot{Q}J + Q\dot{J})B_{G1A,i} + (QJ)C_{G1A,i}\right]_{ret} du_1 du_2 \tag{21}$$

$$A_{G1A,i} = R(0,1)A_{G1,i} \qquad B_{G1A,i} = R(0,1)(\dot{A}_{G1,i} + B_{G1,i}) \qquad C_{G1A,i} = R(0,1)\dot{B}_{G1,i}$$

$$\begin{aligned} 4\pi \frac{c_\infty}{\rho_\infty}\frac{\partial p'_m}{\partial x_i}(x_i,t) = -\int_{\mathrm{f}=0}\Big[&(\dddot{\Lambda}K + 3\ddot{\Lambda}\dot{K} + 3\dot{\Lambda}\ddot{K} + \Lambda\dddot{K})\mathrm{A}_{G1A,i} + \\ &(\ddot{\Lambda}K + 2\dot{\Lambda}\dot{K} + \Lambda\ddot{K})\mathrm{B}_{G1A,i} + (\dot{\Lambda}K + \Lambda\dot{K})\mathrm{C}_{G1A,i} + (\Lambda K)\mathrm{D}_{G1A,i}\Big]_{ret} du \end{aligned} \tag{22}$$

$$\mathrm{A}_{G1A,i} = R(0,1)\mathrm{A}_{G1,i} \qquad \mathrm{B}_{G1A,i} = R(0,1)(\dot{\mathrm{A}}_{G1,i} + \mathrm{B}_{G1,i}) \qquad \mathrm{C}_{G1A,i} = R(0,1)(\dot{\mathrm{B}}_{G1,i} + \mathrm{C}_{G1,i})$$

$$\mathrm{D}_{G1A,i} = R(0,1)\dot{\mathrm{C}}_{G1,i}$$

C. Velocity Formulations

The most recent formulation implemented in ANOPP2 is the velocity formulation, V1A.[29] This formulation provides the acoustic velocity at an observer position. The non-compact and compact forms of the monopole component of Formulation V1A are shown in Eq. 23 and 24, respectively.

$$4\pi\rho_\infty c_\infty u'_{i,m}(x_i,t) = \int_{f=0}\left[(\dot{Q}J + Q\dot{J})A_{V1A,i} + (QJ)B_{V1A,i}\right]_{ret} du_1 du_2 \tag{23}$$

$$A_{V1A,i} = R(0,1)A_{G0,i} \qquad B_{V1A,i} = R(0,1)\dot{A}_{G0,i} + B_{G0,i}$$

$$4\pi c_\infty u'_{i,m}(x_i,t) = \int_{\mathrm{f}=0}\left[(\ddot{\Lambda}K + 2\dot{\Lambda}\dot{K} + \Lambda\ddot{K})\mathrm{A}_{V1A,i} + (\dot{\Lambda}K + \Lambda\dot{K})\mathrm{B}_{V1A,i} + (\Lambda K)\mathrm{C}_{V1A,i}\right]_{ret} du \tag{24}$$

$$\mathrm{A}_{V1A,i} = R(0,2)\mathrm{A}_{G0,i} \qquad \mathrm{B}_{V1A,i} = R(0,1)\dot{R}(0,1)\mathrm{A}_{G0,i} + R(0,1)\mathrm{B}_{G0,i}$$

$$\mathrm{C}_{V1A,i} = R(0,2)\ddot{\mathrm{A}}_{G0,i} + R(0,1)\dot{R}(0,1)\dot{\mathrm{A}}_{G0,i} + R(0,1)\dot{\mathrm{B}}_{G0,i}$$

III. Demonstration

This section demonstrates the compact forms of the formulations by predicting the noise from a wing with constant airfoil cross section undergoing forward flight at three different Mach numbers and a rotorcraft undergoing forward flight at two different advance ratios.

A. Rectilinear Flight

The first example includes a wing with NACA 23012 airfoil cross section at zero angle of attack undergoing forward flight at Mach numbers of 0.25, 0.75, and 0.95. The wing is 10 meters in span with a 0.5 meter chord length. There are two stationary observer positions: directly below the flight path and to the side when $\tau = 0$. The observers are 7.5 meters below and 7.5 meters to the side of the center of the wing at the closest point, shown in Fig. 2. Figure 3 shows the acoustic pressure from the compact and non-compact forms of the time-domain pressure formulations (Formulation 1 and 1A). The differences are negligible. Figure 4 shows the power spectral density from the compact and non-compact forms of Formulation 1, 1A, and 2B. The differences in the compact and non-compact forms are only apparent at the higher bin frequencies, above 100 Hz, when the wing is moving at Mach 0.75 and 0.95. Figure 5 shows the compact and non-compact forms of Formulation V1A. The observer directly below the flight path results in an X_2 component of 0, and the observer to the side results in an X_3 component of 0 and are therefore not shown due to the symmetry of the set up. The differences between the compact and non-compact results are negligible. Figures 6 and 7 show the compact and non-compact forms of the pressure gradient formulations. Similar to the other time-domain formulations, the differences are very small.

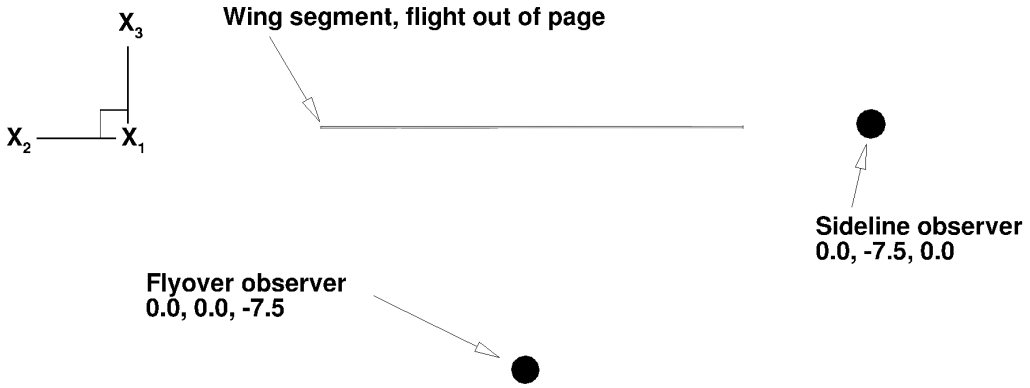

Figure 2. Schematic of wing segment and observer positions. Wing segment moving out of page centered at (0.0, 0.0, 0.0); sideline observer at (0.0, -7.5, 0.0); flyover observer at (0.0, 0.0, -7.5).

B. Rotor

The second demonstration case presented here is a rotor with 4 blades that have NACA 0012 airfoil cross sections undergoing forward flight at two advance ratios. The radius of the rotor is ten meters, and each blade has a chord length of 0.5 meters. The rotation rate and forward flight speed are specified such that the advancing tip Mach numbers are 0.76 and 0.9. The observer positions are 100 meters from the rotor hub in the tip path plane of the rotor. The observers are moving at the same forward speed as the rotor. Figure 8 shows the acoustic pressure time history at 8 observer positions around the rotor when the rotor is moving at an advance ratio of 0.1 with an advancing tip Mach number of 0.76. For brevity, only the non-compact and compact forms of Formulation 1A are shown. The differences between the compact and non-compact forms are extremely small. Figure 9 shows the acoustic pressure for the same observer positions but for a rotor moving at an advance ratio of 0.3 with an advancing tip Mach number of 0.9. For most observer positions the differences between the acoustic pressure predicted by the compact and non-compact formulations are very small. The exceptions are at observer positions directly ahead of the rotor ($\Psi = 135^o, 180^o,$ and 225^o). At these observer positions, the compact form overpredicts the negative peak. Figure 10 shows the power spectral density at the same observer positions as Fig. 9. While the noise at the lower frequencies, where it is the strongest, is predicted well, the prediction by the compact form of Formulation 1A falls off at a different rate when compared to the non-compact form. As a result, the higher frequencies are overpredicted.

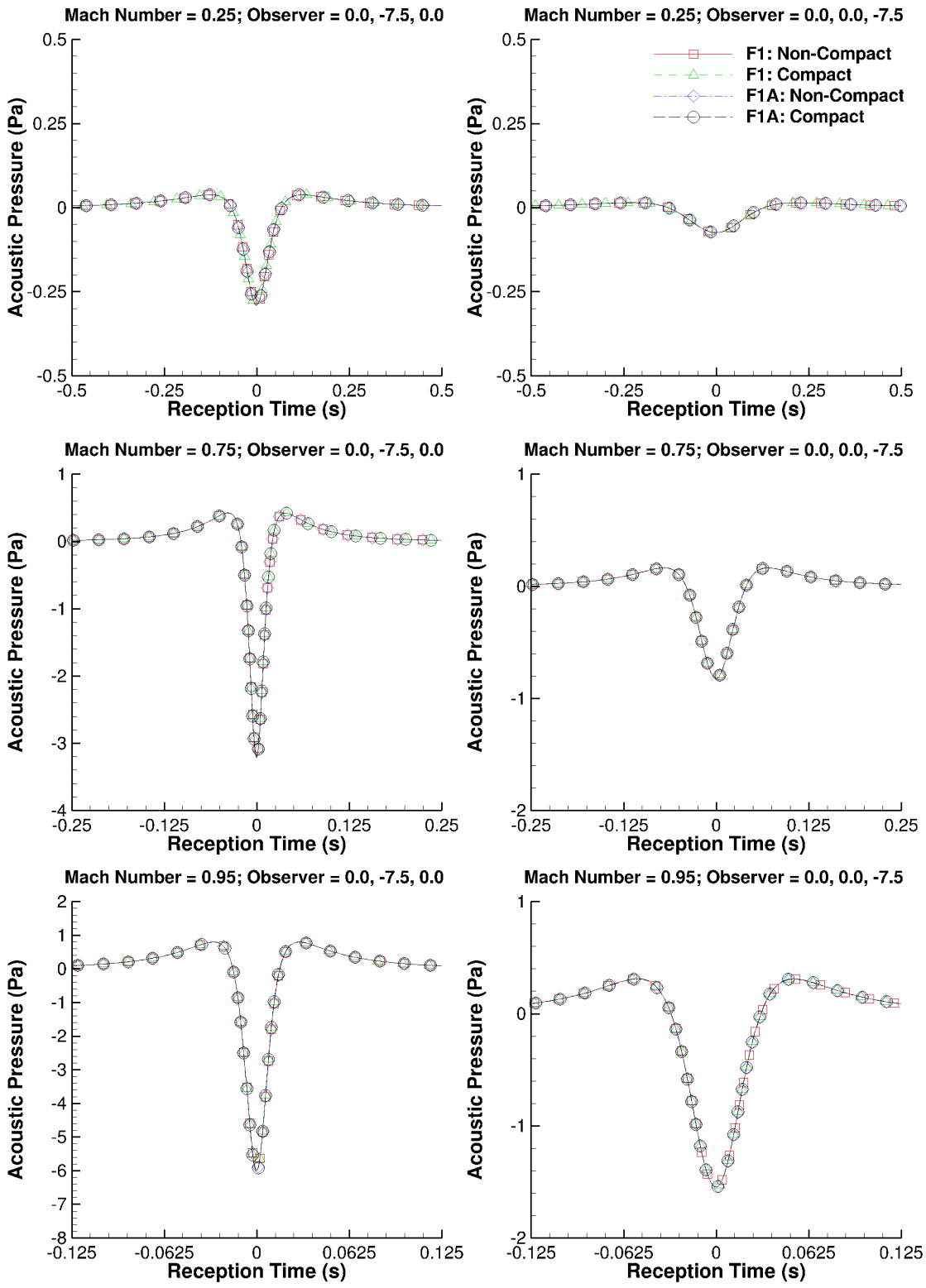

Figure 3. Acoustic pressure time history predicted by non-compact and compact forms of Formulations 1 and 1A. Sideline observer shown in left column and flyover observer shown in right column.

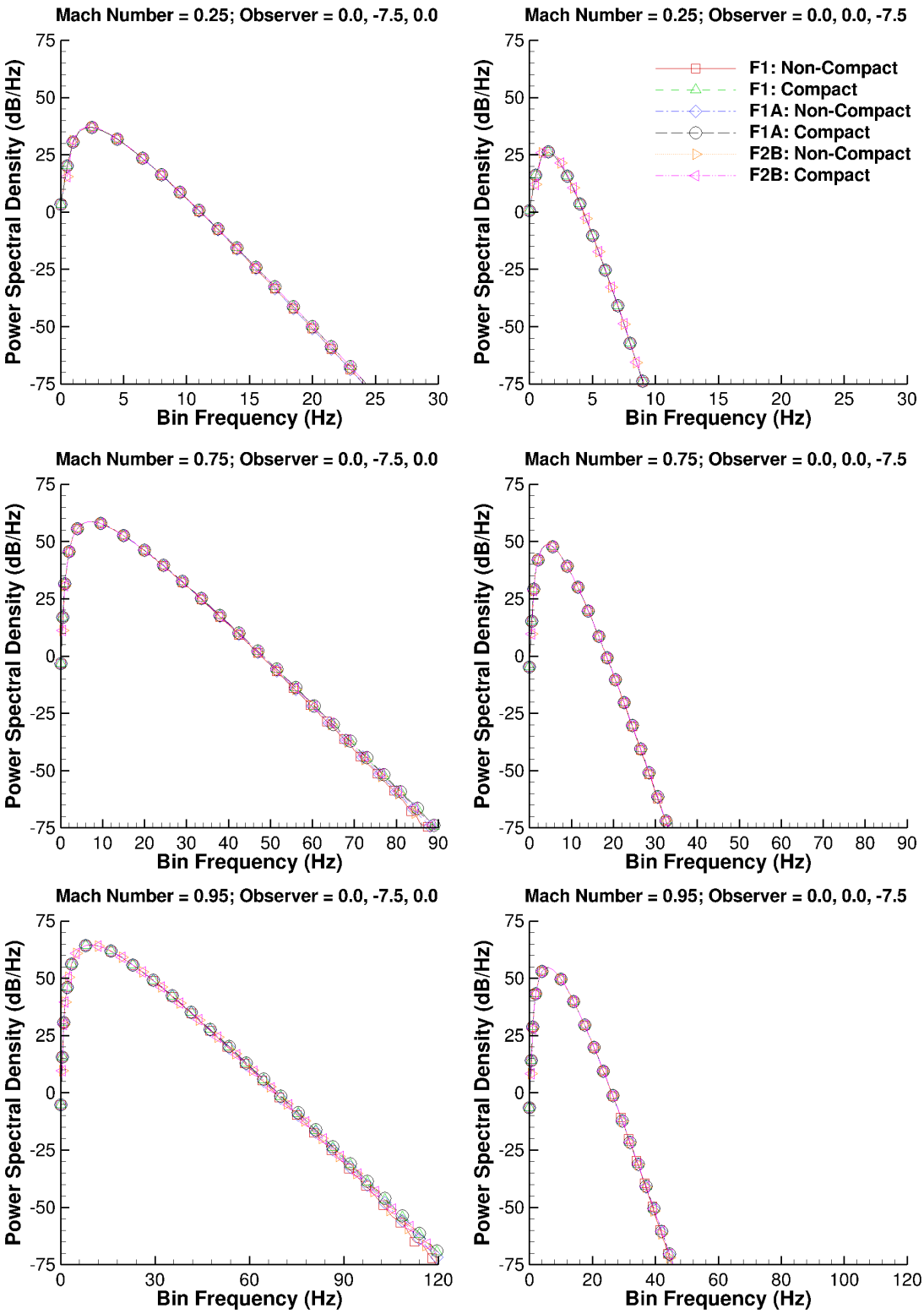

Figure 4. Power spectral density predicted by non-compact and compact forms of Formulations 1, 1A, and 2B. Sideline observer shown in left column and flyover observer shown in right column.

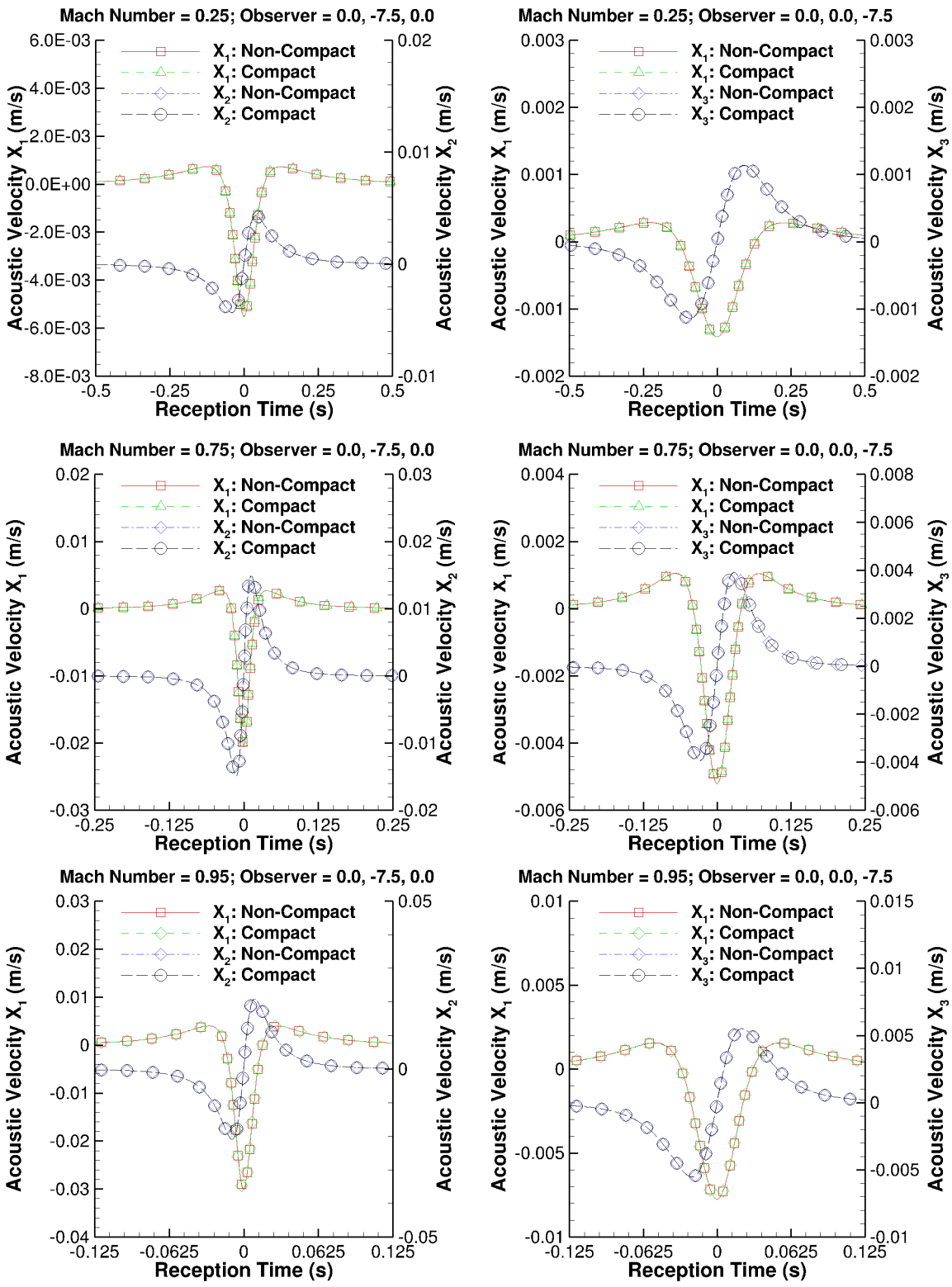

Figure 5. Acoustic velocity predicted by non-compact and compact forms of Formulation V1A. X_1 and X_2 components for sideline (left column) and X_1 an d X_3 components for flyover (right column) observer positions.

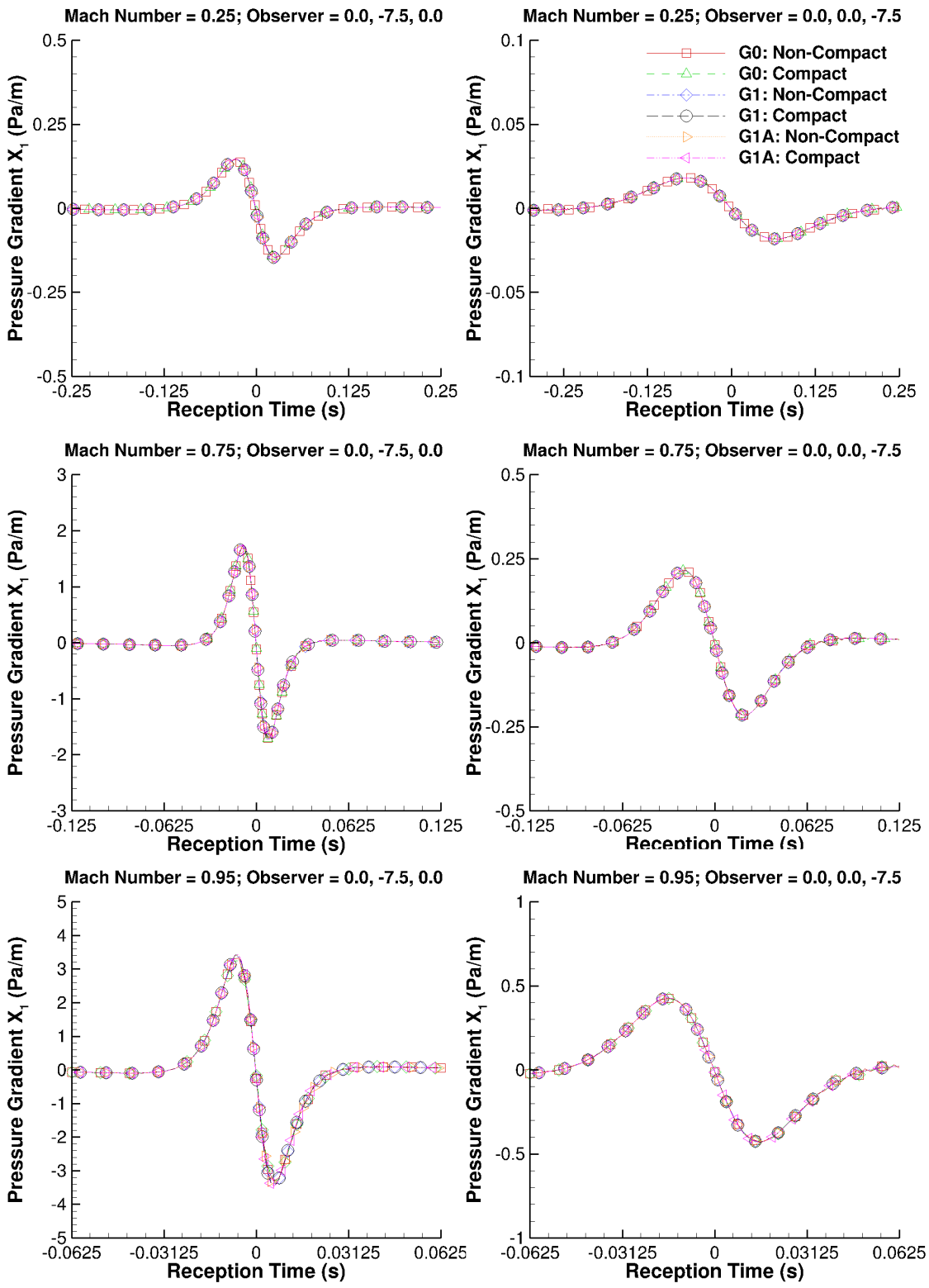

Figure 6. Pressure gradient predicted by non-compact and compact forms of Formulations G0, G1, and G1A. X_1 component for sideline (left column) and flyover (right column) observer positions.

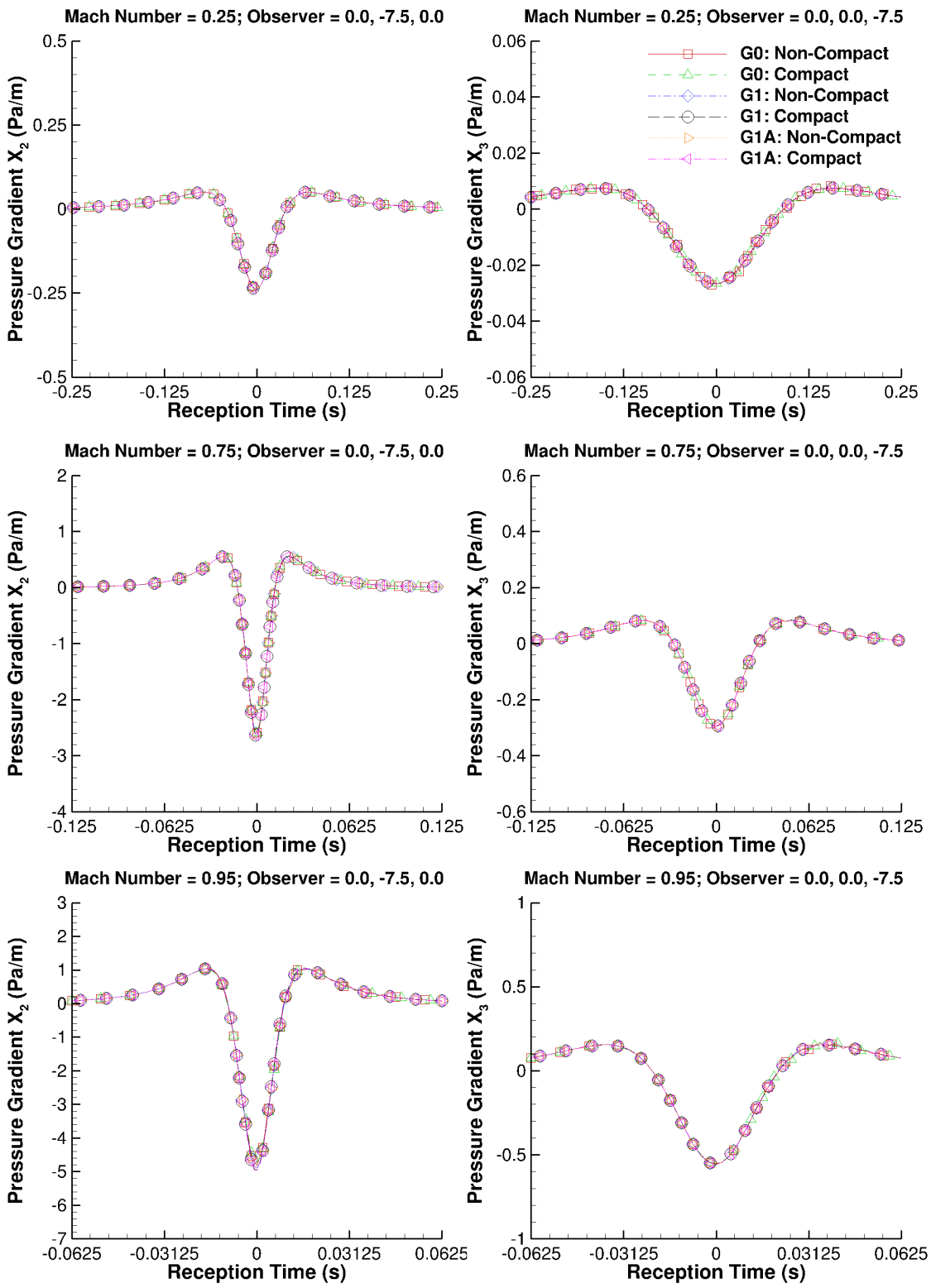

Figure 7. Pressure gradient predicted by non-compact and compact forms of Formulations G0, G1, and G1A. X_2 and X_3 component for sideline (left column) and flyover (right column) observer positions.

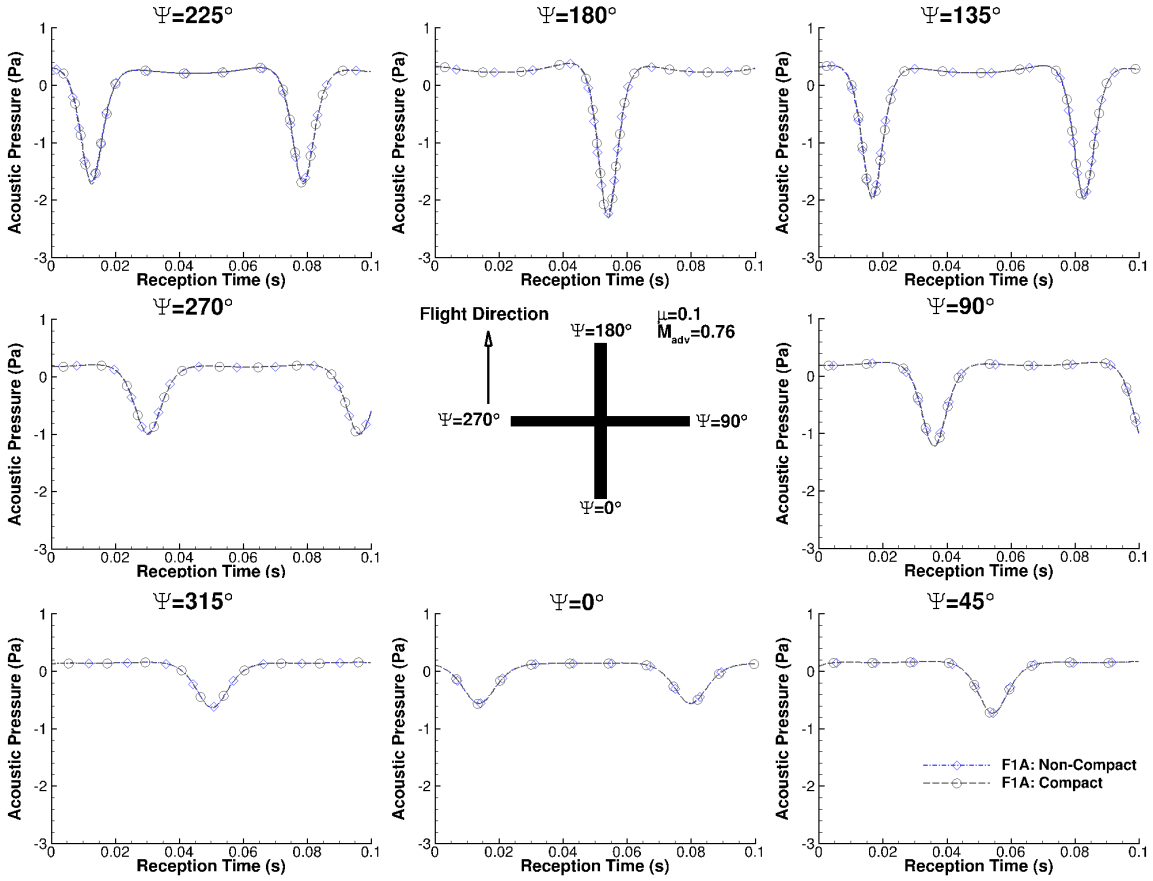

Figure 8. Acoustic pressure time history predicted by non-compact and compact forms of Formulation 1 and 1A at in-plane observer positions. Advance ratio of 0.1 and advancing tip Mach number of 0.76.

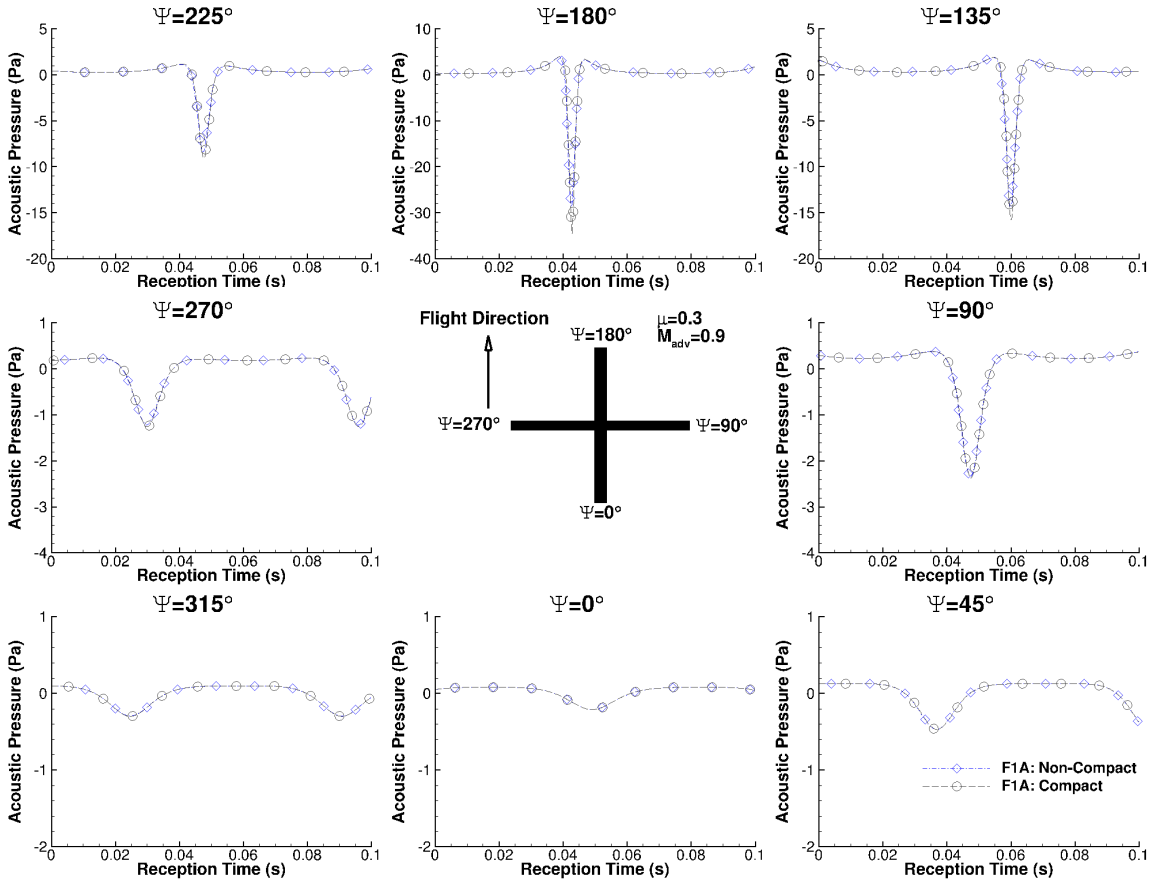

Figure 9. Acoustic pressure time history predicted by non-compact and compact forms of Formulation 1 and 1A at in-plane observer positions. Advance ratio of 0.3 and advancing tip Mach number of 0.9.

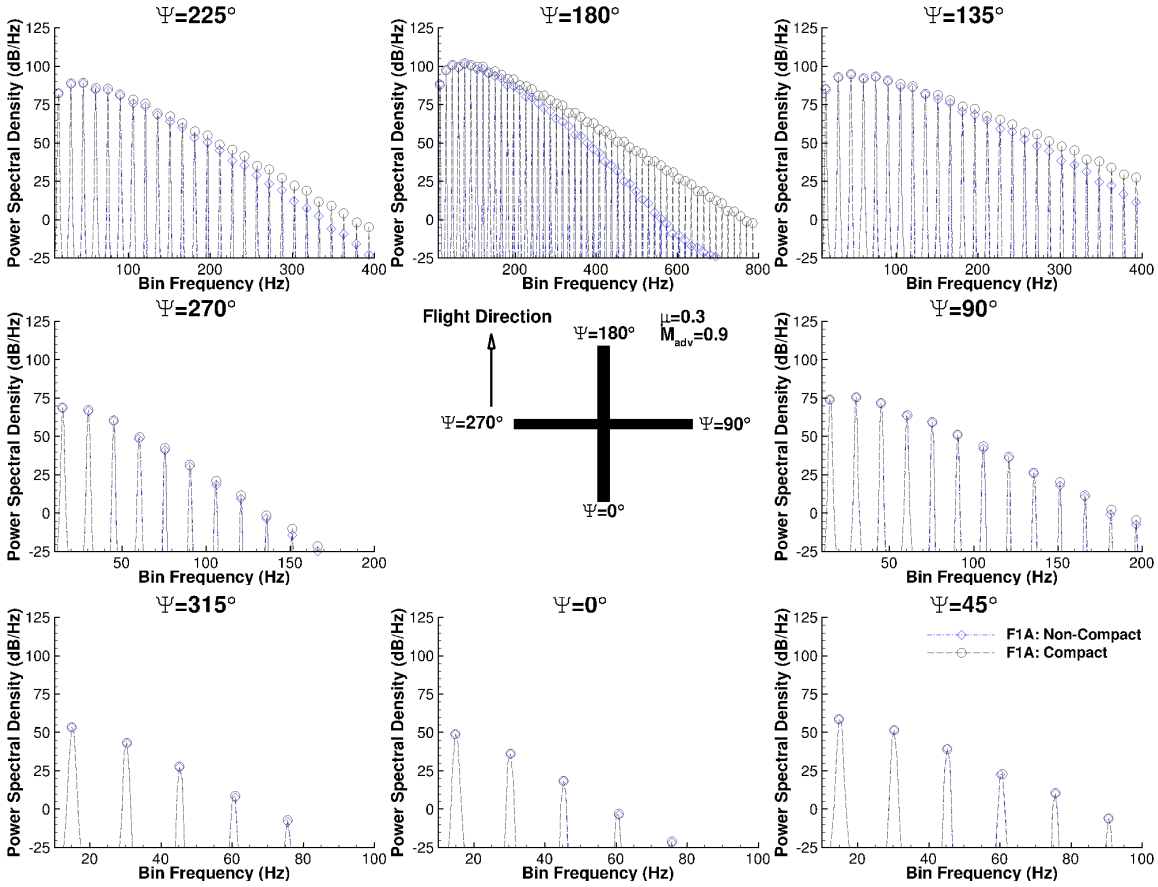

Figure 10. Power spectral density predicted by non-compact and compact forms of Formulation 1A at in-plane observer positions.

The error incurred by using the compact formulation can be seen by analyzing the difference in the Overall Sound Pressure Level (OASPL) between the non-compact and compact forms of Formulation 1A. Table 1 shows the OASPL from the non-compact and compact forms of Formulation 1A at the eight in-plane observer positions around the rotor with an advance ratio of 0.3. The observer position directly in front of the rotor contains the highest amount of error at 0.82dB. The second and third highest errors are at $\Psi = 225^o$and 135^o, respectively.

Table 1. Overall Sound Pressure Level (OASPL) at different in-plane microphone positions for non-compact and compact forms of Formulation 1A. Change in levels (non-compact minus compact) also shown. Isolated rotor at advance ratio of 0.3 and tip Mach number of 0.9.

Ψ	0^o	45^o	90^o	135^o	180^o	225^o	270^o	315^o
Non-Compact	73.79	79.49	90.57	102.91	107.65	99.16	86.05	76.18
Compact	73.79	79.44	90.57	103.26	108.47	99.57	86.24	76.28
Δ dB	0.00	0.04	0.00	-0.34	-0.82	-0.40	-0.19	-0.10

Figure 11 shows the acoustic pressure predicted by the non-compact and compact forms of Formulation 1A over a polar arc directly below the rotor (advance ratio of 0.3 and advancing tip Mach number of 0.9). Similar to the in-plane results, the the out-of-plane results match very closely with the exception of the forward observer location ($\Theta = 15^o$). Table 2 tabulates the differences in OASPL between the two forms for the observer positions below the rotor. Only at an observer positions of $\Theta = 105^o$ are the levels significant; however, at this observer position the levels are extremely small and the differences are primarily a numerical artifact.

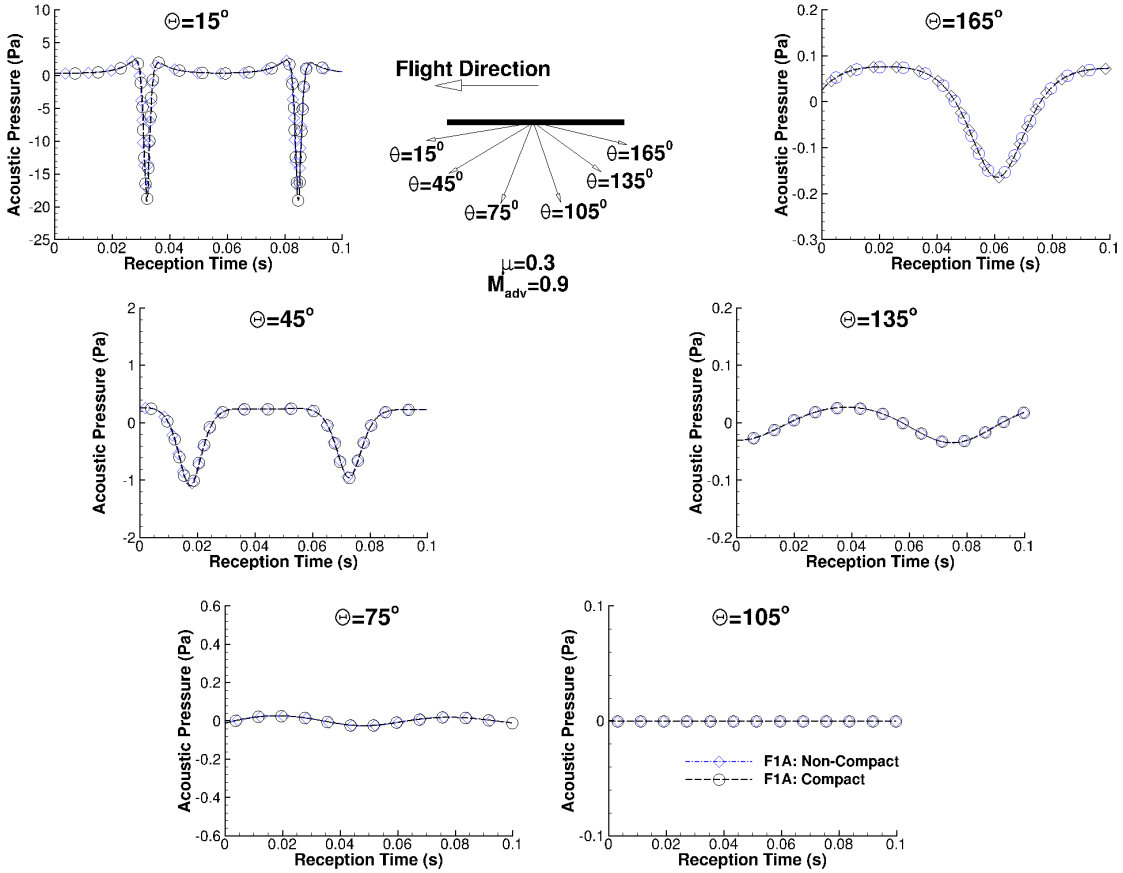

Figure 11. Acoustic pressure time history predicted by non-compact and compact forms of Formulation 1A at out-of-plane observer positions. Rotor is advancing at a ratio of 0.3 with a tip Mach number of 0.9.

Table 2. Overall Sound Pressure Level (OASPL) at different out-of-plane microphone positions for non-compact and compact forms of Formulation 1A. Change in levels (non-compact minus compact) also shown. Isolated rotor at advance ratio of 0.3 and tip Mach number of 0.9.

θ	15^o	45^o	75^o	105^o	135^o	165^o
Non-Compact	104.14	86.38	61.04	23.11	59.83	72.39
Compact	104.65	86.45	61.06	23.84	59.80	72.38
Δ dB	-0.51	-0.07	-0.02	-0.73	0.03	0.00

IV. Blade Shape Study

The compact form of the monopole term of Farassat's formulations is based on the cross sectional area of the airfoil. It is easy to imagine two airfoils with the same cross sectional area which would generate significantly different noise when in motion. In this section, the effect of cross sectional shape on the PSD of the thickness noise emanating from a rotor is studied. Figure 12 shows seven different airfoils with the same cross sectional area ranging from a NACA 0009 to a high aspect ratio, vertically-elongated rectangle, labeled here as Box. Figure 13 shows the compact and non-compact thickness noise predictions using Formulation 1A at an observer directly ahead ($\Psi = 180^o$) of a rotor with an advance ratio of 0.3 and advancing tip Mach number of 0.9. The predictions in Fig. 13 are for rotors with the blade cross sectional shapes outlined in Fig. 12. Regardless of the cross sectional shape, the compact form predicts the same noise because the cross sectional area is the same, and therefore, only one compact prediction is shown. While the peaks at the lower frequencies are well predicted by the compact form, the fall off rate at the high frequencies is significantly different between cross sectional shapes, and the compact form does not predict the fall off rate well. In fact, the compact form predicts the lowest fall off rate while the more elongated blades exhibit faster fall off rates when using the non-compact form. When the compact assumption is applied, the lack of an exact retarded time computation results in all sound sources within the blade being correlated and arriving at the observer at the same time. Higher aspect ratio airfoils, such as the 0009, have a faster fall off rate of sound with increasing frequency because of cancellation due to uncorrelated sources. Conversely, airfoils with low aspect ratio, such as the Box, have a slower fall off rate and therefore are much closer to the compact prediction.

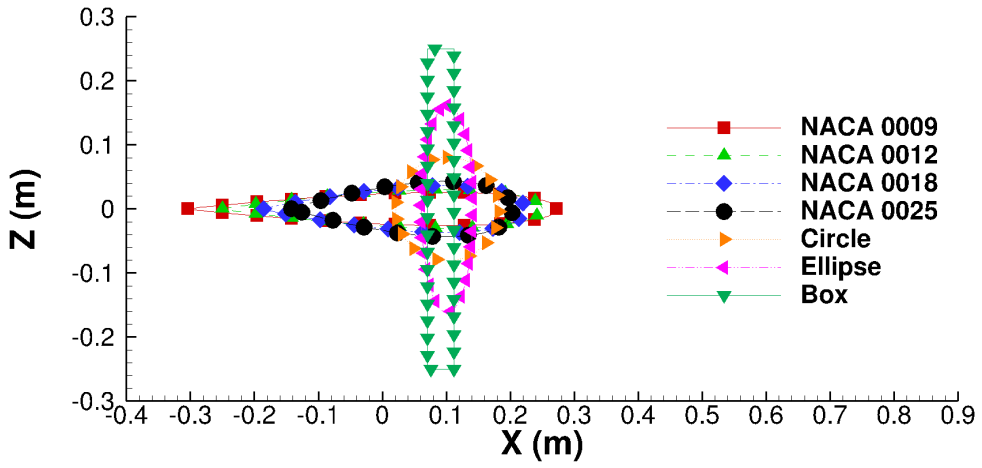

Figure 12. Seven airfoils with the same cross sectional area. The compact form of the thickness term of Farassat's formulations will predict the same noise for each of these airfoils.

Since the fall off rate of sound with respect to frequency for all compact sources is the same regardless of blade shape, it is possible to determine a correction to the noise that can be applied to account for the errors incurred by the compact assumption. Figure 14 shows the change in Overall Sound Pressure Level (OASPL)

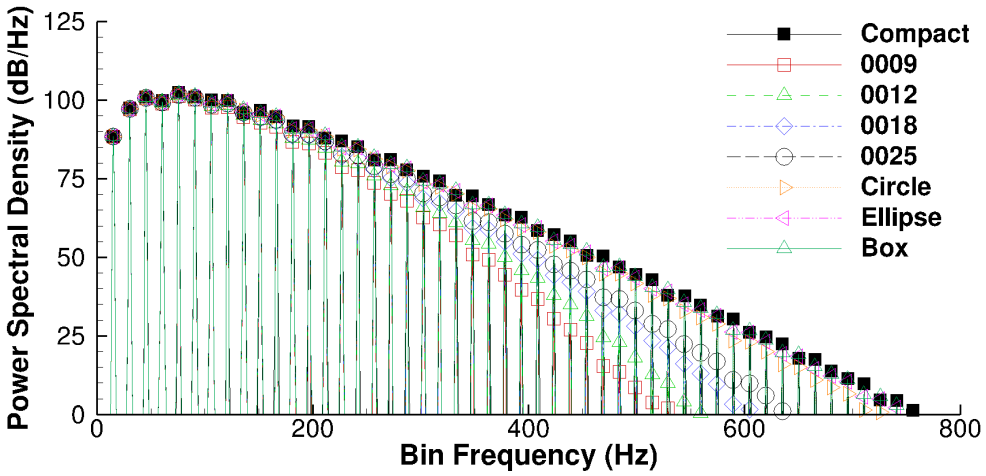

Figure 13. Predictions ahead of a rotor ($\Psi = 180^o$) with different cross sectional shapes and same cross sectional area.

as a function of aspect ratio of the blade cross section. A-weighted OASPL is also shown to demonstrate the influence of frequency weighting to the correction factor. Since the loss of accuracy is frequency dependent, and the lower frequencies contain less error, the curves are have significantly different fall off rates. Using this information, a robust corrective method could easily be determined due to the predictability of the error as a function of azimuth angle and blade shape.

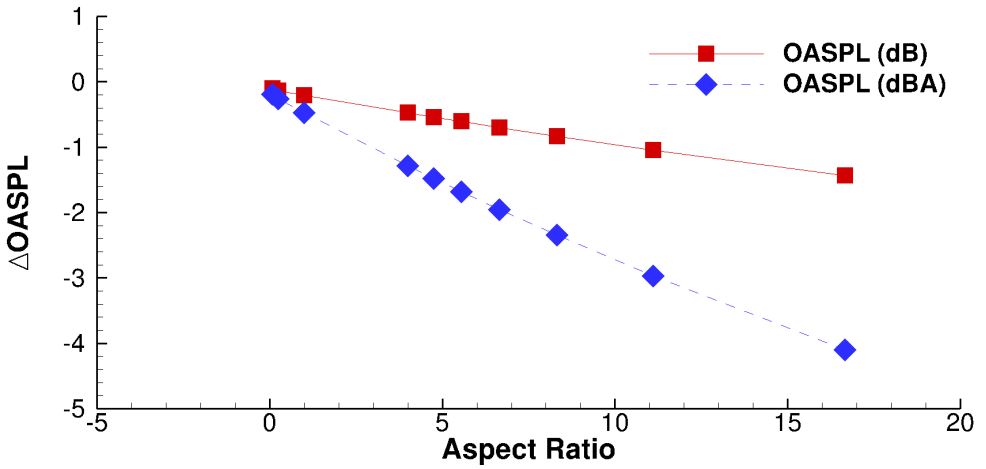

Figure 14. Change in Overall Sound Pressure Level (OASPL) and A-weighted OASPL at $\Psi = 180^o$ as a function of blade cross sectional apsect ratio.

V. Computation Time

s The implementation of the non-compact and compact forms of Farassat's formulations in ANOPP2 differ significantly in computation time. The benefit of the compact forms of the implementation is a significant reduction in computation time at the cost of reduced accuracy for higher frequencies. The accuracy of the compact form has been explored in the previous sections. In this section, the benefit will be shown by running the non-compact and compact forms of Formulation G1A to calculate the pressure gradient on a

body in close proximity to a rotor. For this demonstration, the rotor is identical to that used previously in Section III.B with an advance ratio of 0.3 and advancing tip Mach number of 0.9. To demonstrate a typical calculation which may be required to predict the scattering from a rotorcraft body, a circular body that tapers off sinusoidally toward the front and back is placed 5 meters below the center of the rotor. The body is 20 meters in length and 5 meters in width at its widest point and contains 10201 observer positions. 10201 observers were chosen arbitrarily for demonstration (101 by 101), but should be chosen to capture a specific frequency of scattered sound in practical applications. Figure 15 shows a snapshot in time of the pressure gradient, colored by pressure gradient magnitude, on the rotorcraft body at 2 different viewing angles. The computation time for this calculation on a standard multi-thread capable workstation using the non-compact formulation was approximately 19836 minutes[a] vs. 73 minutes for the compact form on a single computational thread. This represents a 99.6% reduction in computation time.

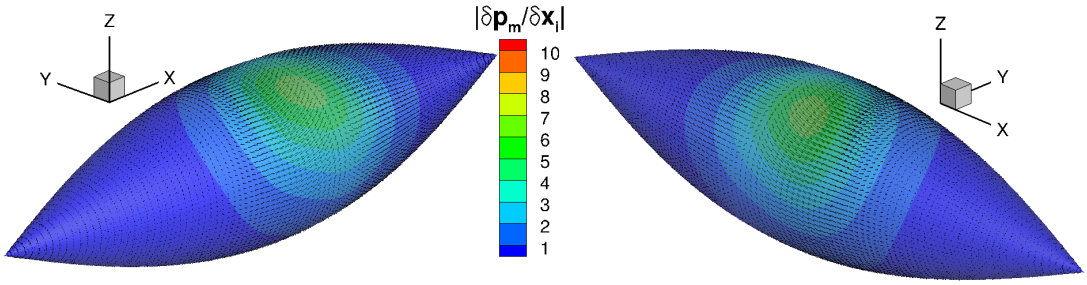

Figure 15. Two views of pressure gradient predicted by compact form of the thickness term of Formulation G1A on body below rotor.

VI. Conclusion

This paper presented and demonstrated compact forms of the monopole term of several of Farassat's formulations including Formulation 1, 1A, G0, G1, G1A, V1A, and 2B. The compact forms of the monopole term were shown to be a function of the blade cross sectional area, reducing the computation from an integration on a surface to an integration along a line. At the cost of slightly reduced accuracy at high tip Mach numbers when not applying any correction, this significantly reduces computation time, facilitating coupling this form of Farassat's Formulations with a design environment such as Model Center or OpenMDAO. The compact forms of all formulations, implemented in ANOPP2, were applied to two example cases: a short span wing with constant airfoil cross section at three forward flight Mach numbers and a rotor undergoing forward flight at two advance ratios. Acoustic pressure time histories of monopole noise predicted from the compact forms of all the formulations at several observer positions were shown to compare very closely to the predictions from their non-compact counterparts. Power spectral densities were also compared to their non-compact counterparts for select formulations and observer positions and shown to match very closely in most cases.

VII. Acknowledgements

This work was funded by NASA's Transformational Tools and Technologies Project in the Transformative Aeronautics Concepts Program and by NASA's Revolutionary Vertical Lift Technology Project in the Advanced Air Vehicles Program.

References

[1] "Aviation and the Environment: Airport Operations and Future Growth Present Environmental Challenges," Tech. Rep. GAO/RCED-00-153, United States General Accounting Office, Washington, D.C. 20548, August 2000.

[a] This computation time was estimated by running the computation for 17.5 hours then extrapolating to calculate a total computation time.

[2]Thomas, R. H., Burley, C. L., and Olson, E. D., "Hybrid Wing Body Aircraft System Noise Assessment With Propulsion Airframe Aeroacoustic Experiments," June 7–9 2010, AIAA Paper No. 2010-3913, presented at the 16^{th} AIAA/CEAS Aeroacoustics Conference.

[3]Thomas, R. H., Burley, C. L., Lopes, L. V., Bahr, C. J., Gern, F. H., and Zante, D. E. V., "System Noise Assessment and the Potential for Low Noise Hybrid Wing Body Aircraft with Open Rotor Propulsion," January 13–17 2014, AIAA Paper No. 2014-0258, presented at the 52^{nd} AIAA/CEAS Aerosciences Meeting.

[4]Raney, J. P., "Development of a New Computer System for Aircraft Noise Prediction," March 24–26 1975, AIAA Paper No. 75-536, presented at the 2^{nd} Aero-acoustics Conference.

[5]Zorumski, W. E., "Aircraft Noise Prediction Program Theoretical Manual, Parts 1 and 2," Tech. Rep. NASA/TM-83199-PT-1 and PT-2, National Aeronautics and Space Administration, Langley Research Center, Hampton, VA., February 1982.

[6]Lopes, L. V. and Burley, C. L., "Design of the Next Generation Aircraft NOise Prediction Program: ANOPP2," AIAA-2011-2854, 17^{th} AIAA/CEAS Aeroacoustics Conference (32^{nd} AIAA Aeroacoustics Conference), June 5–8 2011.

[7]Gray, J. S., Moore, K. T., and Naylor, B. A., "OPENMDAO: An Open Source Framework for Multidisciplinary Analysis and Optimization," *13th AIAA/ISSMO Multidisciplinary Analysis and Optimization Conference, Fort Worth, TX, AIAA, AIAA-2010-9101*, AIAA, Fort Worth, Texas, August 2010.

[8]Farassat, F., "Linear Acoustic Formulas for Calculation of Rotating Blade Noise," *AIAA Journal*, Vol. 19, No. 9, 1980, pp. 1122–1130.

[9]Johnson, W., "Technology Drivers in the Development of CAMRAD II," American Helicopter Society Aeromechanics Specialists Conference, San Francisco, CA, January 1994.

[10]Boyd, D. D., Burley, C. L., and Conner, D. A., "Acoustic Predictions of Manned and Unmanned Rotorcraft Using the Comprehensive Analytical Rotorcraft Model for Acoustics (CARMA) Code System," January 18–20 2005, presented at the American Helicopter Society International Specialists' Meeting on Unmanned Rotorcraft.

[11]Yang, T., Brentner, K. S., Corle, E. K., and Schmitz, S., May 20–22 2014.

[12]Isom, M. P., "The theory of sound radiated by a hovering transonic helicopter blade," *Polytechnic Institute of New York Report*, Vol. 75, No. 4, 1975.

[13]Succi, G. P., "Design of Quiet Efficient Propellers," *SAE Paper 790584*, 1979.

[14]Ffowcs Williams, J. E. and Hawkings, D. L., "Sound Generated by Turbulence and Surfaces in Arbitrary Motion," *Philosophical Transactions of the Royal Society*, Vol. 264, No. 1151, 1969, pp. 321–342.

[15]Gel'fand, I. M. and Shilov, G. E., *Generalized Functions: Properties and Operations*, Vol. 1, Academic Press, Inc., 11 Fifth Avenue, New York 3, New York, 1964, Translated by Eugene Saletan, Department of Physics, Northeastern University, Boston, Massachusetts.

[16]Lighthill, M. J., "On Sound Generated Aerodynamically, I: General Theory," *Proceedings of the Royal Society. A, Mathematical, Physical, and Engineering Sciences*, Vol. 211, 1952, pp. 564–587.

[17]Lighthill, M. J., "On Sound Generated Aerodynamically, II: Turbulence as a Source of Sound," *Proceedings of the Royal Society. A, Mathematical, Physical, and Engineering Sciences*, Vol. 222, 1954, pp. 1–32.

[18]Morgans, A. S., Karabasov, S. A., Dowling, A. P., and Hynes, T. P., "Transonic Helicopter Noise," *AIAA Journal*, Vol. 43, No. 7, 2005, pp. 1512–1524.

[19]Spalart, P. R., Travin, A. L., Shur, M. L., and Strelets, M. K., "Initial Noise Predictions for Open Rotors Using First Principles," AIAA-2010-3793, 16^{th} AIAA/CEAS Aeroacoustics Conference, June 7–9 2010.

[20]Lockard, D. P., Khorrami, M. R., and Li, F., "Aeroacoustic Analysis of a Simplified Landing Gear," AIAA-2003-3111, 10^{th} AIAA/CEAS Aeroacoustics Conference, May 10–13 2004.

[21]Khorrami, M. R. and Bekman, M. E., "Time-Accurate Simulations and Acoustic Analysis of Slat Free-Shear Layer," AIAA-2001-2155, 7^{th} AIAA/CEAS Aeroacoustics Conference, May 28–30 2001.

[22]Wolf, W. R. and Lele, S. K., "Trailing Edge Noise Predictions Using Compressible LES and Acoustic Analogy," AIAA-2011-2784, 17^{th} AIAA/CEAS Aeroacoustics Conference (32^{nd} AIAA Aeroacoustics Conference), June 5–8 2011.

[23]Shur, M. L., Spalart, P. R., Strelets, M. K., and Travin, A. K., "Towards the prediction of noise from jet engines," *Internation Journal of Heat and Fluid Flow*, Vol. 24, No. 4, August 2003, pp. 551–561.

[24]Morris, P. J., Long, L. N., and Brentner, K. S., "An Aeroacoustic Analysis of Wind Turbines," 42^{nd} AIAA Aerospace Sciences Meeting and Exhibit, January 5–8 2004.

[25]Farassat, F. and Casper, J., "Broadband noise prediction when turbulence simulation is available–Derivation of Formulation 2B and its statistical analysis," *Journal of Sound and Vibration*, Vol. 331, 2012, pp. 2203–2208.

[26]Lee, S., Brentner, K. S., and Farassat, F., "Analytic Formulation and Numerical Implementation of an Acoustic Pressure Gradient Prediction," *Journal of Sound and Vibration*, Vol. 319, No. 3-5, 2009, pp. 1200–1221.

[27]Hennes, C. C. and Brentner, K. S., "The Effect of Blade Deformation on Rotorcraft Acoustics," Presented at the 31^{st} European Rotorcraft Forum, September 13–15 2008.

[28]Tinetti, A. F., Dunn, M. H., and Pope, D. S., *Fast Scattering Code (FSC) User's Manual, Version 2.0*, October 2006, NASA CR 2006-214510.

[29]Ghorbaniasl, G., Carley, M., and Lacor, C., "Acoustic Velocity Formulation for Sources in Arbitrary Motion," *AIAA Journal*, Vol. 51, No. 3, 2013, pp. 632–642.

VIII. Appendix

The dipole term of each formulation (acoustic pressure, pressure gradient, acoustic velocity) implemented in ANOPP2 is presented here.

A. Pressure Formulations

The non-compact and compact forms of the dipole term of Formulation 1 are shown in Eq. 25 and 26, respectively.

$$4\pi c_\infty p'_d(x_i,t) = \frac{\partial}{\partial t}\int\limits_{f=0}\left[(L_i J)B_{1,i}\right]_{ret} du_1 du_2 + \int\limits_{f=0}\left[(L_i J)C_{1,i}\right]_{ret} du_1 du_2 \tag{25}$$

$$B_{1,i} = R(1,1)\hat{r}_i \qquad C_{1,i} = c_\infty R(2,1)\hat{r}_i$$

$$4\pi c_\infty p'_d(x_i,t) = \frac{\partial}{\partial t}\int\limits_{\mathrm{f=0}}\left[(F_i K)\mathrm{B}_{1,i}\right]_{ret} du + \int\limits_{\mathrm{f=0}}\left[(F_i K)\mathrm{C}_{1,i}\right]_{ret} du \tag{26}$$

$$\mathrm{B}_{1,i} = R(1,1)\hat{r}_i \qquad \mathrm{C}_{1,i} = c_\infty R(2,1)\hat{r}_i$$

The non-compact and compact forms of the dipole term of Formulation 1A are shown in Eq. 27 and 28, respectively.

$$4\pi c_\infty p'_d(x_i,t) = \int\limits_{f=0}\left[(\dot{L}_i J + L_i \dot{J})C_{1A,i} + (L_i J)D_{1A,i}\right]_{ret} du_1 du_2 \tag{27}$$

$$C_{1A,i} = R(0,1)B_{1,i} \qquad D_{1A,i} = R(0,1)\dot{B}_{1,i} + C_{1,i}$$

$$4\pi c_\infty p'_d(x_i,t) = \int\limits_{\mathrm{f=0}}\left[(\dot{F}_i K + F_i \dot{K})\mathrm{D}_{1A,i} + (F_i K)\mathrm{E}_{1,i}\right]_{ret} du \tag{28}$$

$$\mathrm{D}_{1A,i} = R(0,1)\mathrm{B}_{1,i} \qquad \mathrm{E}_{1A,i} = R(0,1)\dot{\mathrm{B}}_{1,i} + \mathrm{C}_{1,i}$$

The non-compact and compact forms of the dipole term of Formulation 2B are shown in Eq. 29 and 30, respectively.

$$4\pi\rho_\infty c_\infty \Phi_d(x_i,t) = -\int\limits_{f=0}\left[(L_i J)B_i\right]_{ret} du_1 du_2 - \int_{-\infty}^{t}\int\limits_{f=0}\left[(L_i J)C_i\right]_{ret} du_1 du_2 dt' \tag{29}$$

$$B_{2B,i} = R(1,1)\hat{r}_i \qquad C_{2B,i} = c_\infty R(2,1)\hat{r}_i$$

$$4\pi\rho_\infty c_\infty \Phi_d(x_i,t) = -\int\limits_{\mathrm{f=0}}\left[(F_i K)\mathrm{B}_i\right]_{ret} du - \int_{-\infty}^{t}\int\limits_{\mathrm{f=0}}\left[(F_i K)\mathrm{C}_i\right]_{ret} du dt' \tag{30}$$

$$\mathrm{B}_{2B,i} = R(1,1)\hat{r}_i \qquad \mathrm{C}_{2B,i} = c_\infty R(2,1)\hat{r}_i$$

B. Pressure Gradient Formulations

The dipole terms of the non-compact and compact forms of Formulation G0 are shown in Eq. 31 and 32, respectively.

$$\begin{aligned} 4\pi c_\infty^2 \frac{\partial}{\partial x_i} p'_d(x_i,t) = &-\frac{\partial^2}{\partial t^2}\int\limits_{f=0}\left[(L_j J)C_{G0,ij}\right]_{ret} du_1 du_2 + \\ &\frac{\partial}{\partial t}\int\limits_{f=0}\left[(L_j J)D_{G0,ij}\right]_{ret} du_1 du_2 + \int\limits_{f=0}\left[(L_j J)E_{G0,ij}\right]_{ret} du_1 du_2 \end{aligned} \tag{31}$$

$$C_{G0,ij} = R(1,1)\hat{r}_i\hat{r}_j \qquad D_{G0,ij} = c_\infty R(2,1)(\delta_{ij} - 3\hat{r}_i\hat{r}_j) \qquad E_{G0,ij} = c_\infty^2 R(3,1)(\delta_{ij} - 3\hat{r}_i\hat{r}_j)$$

$$\begin{aligned} 4\pi c_\infty^2 \frac{\partial}{\partial x_i} p'_d(x_i,t) = &-\frac{\partial^2}{\partial t^2}\int\limits_{\mathrm{f=0}}\left[(F_j K)\mathrm{C}_{G0,ij}\right]_{ret} du_1 du_2 + \frac{\partial}{\partial t}\int\limits_{\mathrm{f=0}}\left[(F_j K)\mathrm{D}_{G0,ij}\right]_{ret} du_1 du_2 + \\ &\int\limits_{\mathrm{f=0}}\left[(F_j K)\mathrm{E}_{G0,ij}\right]_{ret} du_1 du_2 \end{aligned} \tag{32}$$

$$\mathrm{C}_{G0,ij} = R(1,1)\hat{r}_i\hat{r}_j \qquad \mathrm{D}_{G0,ij} = c_\infty R(2,1)(\delta_{ij} - 3\hat{r}_i\hat{r}_j) \qquad \mathrm{E}_{G0,ij} = c_\infty^2 R(3,1)(\delta_{ij} - 3\hat{r}_i\hat{r}_j)$$

The dipole terms of the non-compact and compact forms of Formulation G1 are shown in Eq. 33 and 34, respectively.

$$\begin{aligned} 4\pi c_\infty^2 \frac{\partial}{\partial x_i} p'_d(x_i,t) = &- \frac{\partial}{\partial t}\left\langle \int\limits_{f=0} \left[(\dot{L}_j J + L_j \dot{J}) C_{G1,ij} + (L_j J) D_{G1,ij} \right]_{ret} du_1 du_2 \right\rangle + \\ &\int\limits_{f=0} \left[(L_j J) E_{G1,ij} \right]_{ret} du_1 du_2 \end{aligned} \tag{33}$$

$$C_{G1,ij} = R(0,1)C_{G0,ij} \qquad D_{G1,ij} = R(0,1)\dot{C}_{G0,ij} - D_{G0,ij} \qquad E_{G1,ij} = E_{G0,ij}$$

$$4\pi c_\infty^2 \frac{\partial}{\partial x_i} p'_d(x_i,t) = -\frac{\partial}{\partial t}\left\langle \int\limits_{\mathrm{f}=0} \left[(\dot{F}_j K + F_j \dot{K})\mathrm{D}_{G1,ij} + (F_j K)\mathrm{E}_{G1,ij} \right]_{ret} du \right\rangle + \int\limits_{\mathrm{f}=0} \left[(F_j K)\mathrm{F}_{G1,ij} \right]_{ret} du \tag{34}$$

$$\mathrm{D}_{G1,ij} = R(0,1)\mathrm{C}_{G0,ij} \qquad \mathrm{E}_{G1,ij} = R(0,1)\dot{\mathrm{C}}_{G0,ij} - \mathrm{D}_{G0,ij} \qquad \mathrm{F}_{G1,ij} = \mathrm{E}_{G0,ij}$$

The dipole terms of the non-compact and compact forms of Formulation G1A are shown in Eq. 35 and 36, respectively.

$$\begin{aligned} &4\pi c_\infty^2 \frac{\partial}{\partial x_i} p'_d(x_i,t) = \\ &\quad - \int\limits_{f=0} \left[(\ddot{L}_j J + 2\dot{L}_j \dot{J} + L_j \ddot{J}) D_{G1,ij} + (\dot{L}_j J + L_j \dot{J}) E_{G1A,i} + (L_j J) F_{G1A,i} \right]_{ret} du_1 du_2 \end{aligned} \tag{35}$$

$$D_{G1A,ij} = R(0,1)C_{G1,ij} \qquad E_{G1A,ij} = R(0,1)(\dot{C}_{G1,ij} + D_{G1,ij}) \qquad F_{G1A,ij} = R(0,1)\dot{D}_{G1,ij} - E_{G1,ij}$$

$$4\pi c_\infty^2 \frac{\partial}{\partial x_i} p'_d(x_i,t) = -\int\limits_{\mathrm{f}=0} \left[(\ddot{F}_j K + 2\dot{F}_j \dot{K} + F_j \ddot{K})\mathrm{E}_{G1,ij} + (\dot{F}_j K + F_j \dot{K})\mathrm{F}_{G1A,i} + (F_j K)\mathrm{G}_{G1A,i} \right]_{ret} du \tag{36}$$

$$\mathrm{E}_{G1A,ij} = R(0,1)\mathrm{D}_{G1,ij} \qquad \mathrm{F}_{G1A,ij} = R(0,1)(\dot{\mathrm{D}}_{G1,ij} + \mathrm{E}_{G1,ij}) \qquad \mathrm{G}_{G1A,ij} = R(0,1)\dot{\mathrm{E}}_{G1,ij} - \mathrm{F}_{G1,ij}$$

C. Acoustic Velocity Formulations

The dipole terms of the non-compact and compact forms of Formulation V1A are shown in Eq. 37 and 38, respectively.

$$\begin{aligned} 4\pi\rho_\infty c_\infty^2 u'_{i,d}(x_i,t) = &\int\limits_{f=0} \left[(\dot{L}_j J + L_j \dot{J}) C_{V1A,ij} + (L_j J) D_{V1A,ij} \right]_{ret} du_1 du_2 - \\ &\int_\infty^t \int\limits_{f=0} \left[(L_j J) E_{V1A,ij} \right]_{ret} du_1 du_2 dt' \end{aligned} \tag{37}$$

$$C_{V1A,ij} = R(0,1)C_{G0,ij} \qquad D_{V1A,ij} = R(0,1)\dot{C}_{G0,ij} - D_{G0,ij} \qquad E_{V1A,ij} = E_{G0,ij}$$

$$\begin{aligned} 4\pi\rho_\infty c_\infty^2 u'_{i,d}(x_i,t) = &\int\limits_{\mathrm{f}=0} \left[(\dot{F}_j K + F_j \dot{K})\mathrm{D}_{V1A,ij} + (F_j K)\mathrm{E}_{V1A,ij} \right]_{ret} du - \\ &\int_\infty^t \int\limits_{\mathrm{f}=0} \left[(F_j K)\mathrm{F}_{V1A,ij} \right]_{ret} du dt' \end{aligned} \tag{38}$$

$$\mathrm{D}_{V1A,ij} = R(0,1)\mathrm{C}_{G0,ij} \qquad \mathrm{E}_{V1A,ij} = R(0,1)\dot{\mathrm{C}}_{G0,ij} - \mathrm{D}_{G0,ij} \qquad \mathrm{F}_{V1A,ij} = \mathrm{E}_{G0,ij}$$